Magnetic enhancement of $Co_{0.2}Zn_{0.8}Fe_2O_4$ spinel oxide by mechanical milling

R. N. Bhowmik* and R. Ranganathan†
Experimental Condensed Matter Physics Division, Saha Institute of Nuclear Physics, 1/AF Bidhannagar, Calcutta 700064, India

S. Sarkar and C. Bansal
School of Physics, University of Hyderabad, Hyderabad 500046, India

R. Nagarajan
Tata Institute of Fundamental Research, Mumbai 40005, India

(Received 8 July 2002; revised manuscript received 23 June 2003; published 20 October 2003)

The mechanical milled $Co_{0.2}Zn_{0.8}Fe_2O_4$ spinel oxide with average particle size $\approx$20 nm shows an enhancement in both magnetization (i.e., more ferromagnetic) and ordering temperature comparing the bulk sample. The annealing of the as milled sample at different temperatures starts the grain (particle) growth process and magnetically recovering the bulk properties after heat treatment. As for example, the as milled sample after annealing at $\sim$1273 K for 6 h exhibits two coexisting magnetic states, i.e., cluster spin-glass state and ferrimagnetic state, similar to the as prepared bulk sample. The room-temperature Mössbauer spectra of the as milled sample, annealed at 573 K for different duration (up to 575 h), indicate that the ferromagnetic behavior above room temperature is strongly related to site exchange of cations among tetrahedral (*A*) and octahedral (*O*) sites in the spinel structure. The experimental data also suggest that the lowering of *B* site spin canting and increase of strain induced unidirectional anisotropy by mechanical milling play an important role in controlling the magnetic order of the as milled sample. Importantly, the grain boundary spins of the as milled sample do not show to be magnetically inactive, rather they give rise to a preferential orientation due to strain induced anisotropy.

DOI: 10.1103/PhysRevB.68.134433 PACS number(s): 75.50.Tt, 36.40.Cg, 75.75.+a

I. INTRODUCTION

Nanoparticle spinel oxides are attracting increasing interest in research because of their potential applications in nanoscience and technology[1–3] and also for fundamental understanding of the strikingly different properties of the same material when the particle size approaches the atomic scale level.[4–8] Some of the novel properties in magnetic nanoparticles, such as superparamagnetism, quantum magnetic tunneling, and surface spin canting effect,[1,9,10] have generated further interest in the study of nanoparticle spinels. Among the various kinds of preparation techniques of nanoparticles, mechanical milling has been recognized as a powerful and standard technique for the production of huge quantities of nanoparticle materials. After the discovery of spin-glass behavior in Co_2Ge alloy by Zhou and Bakker,[11] a rich variety of nonequilibrium magnetic states, such as superparamagnetic or superspin glass and so on,[12,13] in mechanical milled nanoparticle is becoming very important to study the nonequilibrium spin dynamics. The enhancement of magnetization and unidirectional anisotropy in mechanical milled spinel oxide[14–16] are further useful to understand the modification of superexchange interactions and grain boundary effects. Besides the magnetic transformation, atomic disorder introduced during mechanical milling has also shown its significant role in the electron scattering at the magnetic and nonmagnetic interfaces and in resulted large giant magnetorsistance in a granular heterogeneous alloy.[5]

In spinel oxide AB_2O_4,[3] the magnetic order depends on the competition between various kinds of superexchange interactions among *A* and *B* site cations, i.e., J_{AB} (*A*-O-*B*), J_{BB} (*B*-O-*B*), and J_{AA}(*A*-O-*A*).[3] Certain amount of site exchange of cations is sufficient to change J_{AB} and J_{BB} interactions and has shown drastically different magnetic behavior in nanoparticle spinel in comparison with the bulk.[17–19] Most of the reports on nanoparticle spinels start with bulk MFe_2O_4 (M = Mn, Zn, Ni, and Co), where magnetic order (ferro/ferri) is of long range with collinear spin structure and J_{AB} are much more stronger than J_{BB}.[6–10] In these spinels, the strong surface spin canting effect occurs when the particle size reduces to nanometer range. The competition between the disordered (canted) surface spins and ordered core spins determines the magnetic ground state and usually exhibits the decrease of magnetization and ordering temperature in nanoparticle spinel.[7,9]

However, the reduction of magnetization and ordering temperature is not the fact for a few mechanical milled nanoparticle spinels such as $ZnFe_2O_4$,[15] $CdFe_2O_4$,[16] and $NiFe_2O_4$.[17] For example, the antiferromagnetic order of bulk $ZnFe_2O_4$ (structure: $(Zn^{2+})_A[Fe_2^{3+}]_BO_4$) below 10 K transforms into ferrimagnetic order even at $T>10$ K with large magnetic moment by mechanical milling. Such a magnetic enhancement in mechanical milled $ZnFe_2O_4$ nanoparticle has been attributed to the exchange of cations (Zn^{2+} and Fe^{3+}) among *A* and *B* sites.[10,15–17] Though magnetic order and magnetization are enhanced in the above-mentioned three mechanical milled spinels, the experimental value of saturation magnetization is well below the expected value. In case of $CdFe_2O_4$, the lower value of experimental finding $\sim$21.7 emu/g at 5 K lower than the expected value $\sim$80 emu/g was attributed to the local spin canting in both *A*

and *B* sites, even after mechanical milling.[16]

The important role of spin canting was realized by the work on a series of bulk $Co_{1-x}Zn_xFe_2O_4$ spinel oxides,[20] where the increase of *B* site spin canting has shown the decrease in magnetization and magnetic order for $x \geqslant 0.6$ samples. The expression for magnetization $M(=M_B\cos\theta - M_A)$ (Ref. 3) suggest that the increase of *A* site magnetic moment M_A should decrease the total magnetization of spinel structure, whereas the associated intersublattice superexchange interactions J_{AB} are increased. In our opinion, the increase of total magnetization in spinel oxides, irrespective of nanocrystalline[10,17] and bulk form, not only depends on the sublattice (site) magnetization M_B and M_A or site exchange of cations, but also largely depends on the decrease of spin canting angle θ between the *B* site spins, which can exhibit both the increase of total magnetization and the ferrimagnetic/ferromagnetic order in spinel oxide. To our knowledge, there is no experimental report which has focussed on the ''inverse of spin canting'' effect, i.e., the reduction of *B* site spin canting leading to the increase of magnetization in nanoparticle spinel.

In this light, we have investigated bulk $Co_{0.2}Zn_{0.8}Fe_2O_4$ spinel oxide with cation distribution $(Zn^{2+}_{0.8}Fe^{+3}_{0.2})_A[Co^{+2}_{0.2}Fe^{3+}_{1.8}]_BO_4$.[21] Because of low *A* site magnetic moment (~ 0.2) and weak J_{AB} interactions, the *B* site spins are canted. Our hypothesis is that only if site exchange of cations are associated with the reduction of *B* site spin canting, enhancement both of magnetization and magnetic order are possible in nanoparticle spinel oxide. In this work, we test this hypothesis by mechanical milling of bulk $Co_{0.2}Zn_{0.8}Fe_2O_4$ and probing the system through magnetization measurements and Mössbauer spectroscopy.

II. EXPERIMENT

Stoichiometric amounts of ZnO, Fe_2O_3, and Co_3O_4 (purity $>99.9\%$) were mixed for $Co_{0.2}Zn_{0.8}Fe_2O_4$ compound and ground for 2 h. The mixture was pelletized and sintered at 1223 K for 12 h and slowly cooled to room temperature. The pellet was again ground, and pelletized and sintered at 1273 K for 12 h. The heat treatment was carried out under atmospheric condition with heating and cooling rate of 2–3 K/min. The x-ray diffraction (XRD) spectrum (Fig. 1) for as prepared bulk (S_0) sample, recorded using Philips PW1710 diffractometer with CuK_α radiation, represents standard polycrystalline structure of cubic spinel phase. The S_0 sample was milled for 24 h in a SPEX 8000 mixer/mill using six balls, two of diameter 1/2 in. and four of diameter 1/4 in. with ball to powder weight ratio 5:1. The x-ray fluorescence spectra of as milled (S_1) sample confirmed no significant contamination from the steel balls ($Fe_{74}Cr_{18}Ni_8$). The XRD spectrum of S_1 sample (Fig. 1) shows that the XRD lines are broad due to smaller particle size, but the spinel structure is retained. The S_1 sample which is annealed at different temperatures (T_{AN}) for 6 h, in separate batches, are denoted as S_{N3} (573 K), S_{N6} (873 K), and S_{N10} (1273 K). The XRD spectra in Fig. 1 show that broad lines of of S_1 sample become narrow with increasing T_{AN} and the samples continue to retain the spinel structure. Using the width of $\langle 311\rangle$ XRD

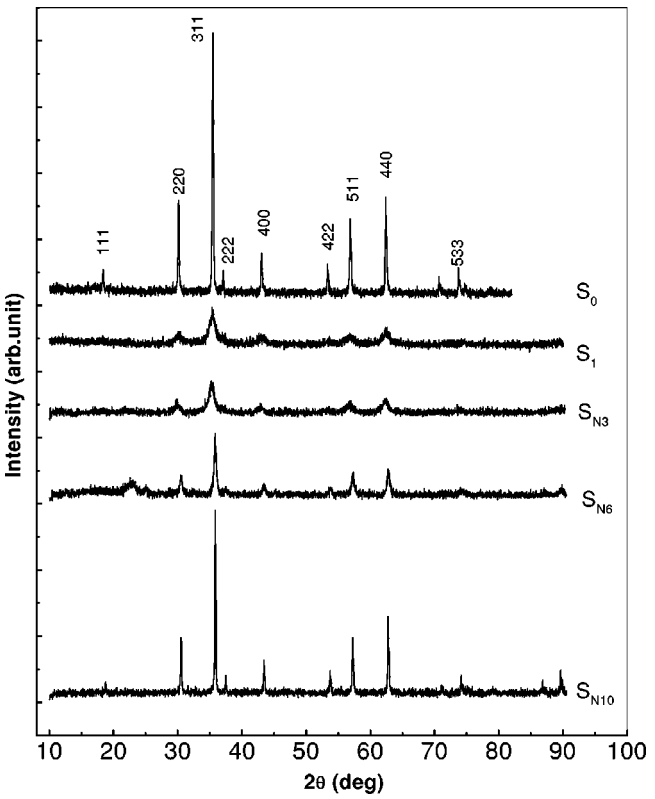

FIG. 1. XRD spectra for $Co_{0.2}Zn_{0.8}Fe_2O_4$ spinel oxide heated at different temperatures. S_0: bulk, S_1: as milled, S_{N3}: 573 K-6 h heat treated, S_{N6}: 873 K-6 h heat treated and S_{N10}: 1273 K-6 h heat treated sample.

peak line, we find that particle size increases with T_{AN} as 20 nm, 23 nm, 28 nm, and 62 nm for the samples S_1, S_{N3}, S_{N6}, and S_{N10}, respectively. Therefore, the increasing sharpness of XRD lines (Fig. 1) indicates that thermal activation energy is monitoring the recrystallization process via grain boundary atomic diffusion.[22] It is to be noted that the XRD spectrum of the S_{N10} sample may be very similar to that of S_0 sample, but its small particle size ≈ 62 nm suggests that complete restoration of crystallinity close to S_0 sample is yet to be reached. To study the temporal phase evolution, S_1 sample was also annealed at 573 K for time (t_{AN}) ranging from 2 h to 575 h.

The low field dc magnetization ($H=10$–100 Oe) under zero-field cooled (ZFC) and field cooled (FC) modes and ac susceptibility [$h_{rms} \approx 1$ Oe and frequency (f) = 337 Hz and 7 kHz] measurements were performed using home made magnetometer.[23] In ZFC (FC) mode, the sample was cooled from 320 K to 20 K in the absence (presence) of dc magnetic field, then the measurement field was applied at 20 K and magnetization data were recorded while increasing the temperature. In FC mode, the cooling field and measurement fields are same in magnitude. High-field (up to ± 12 T) magnetization was measured using vibrating-sample magnetometer. Mössbauer spectra of the samples were recorded at 300 K without applying external magnetic field, using a constant acceleration spectrometer in transmission geometry. The spectra were recorded using a 5-mCi ^{57}Co source in Rh matrix. The hyperfine magnetic-field (HMF) distribution at the ^{57}Fe nuclei was evaluated from the Mössbauer spectra using

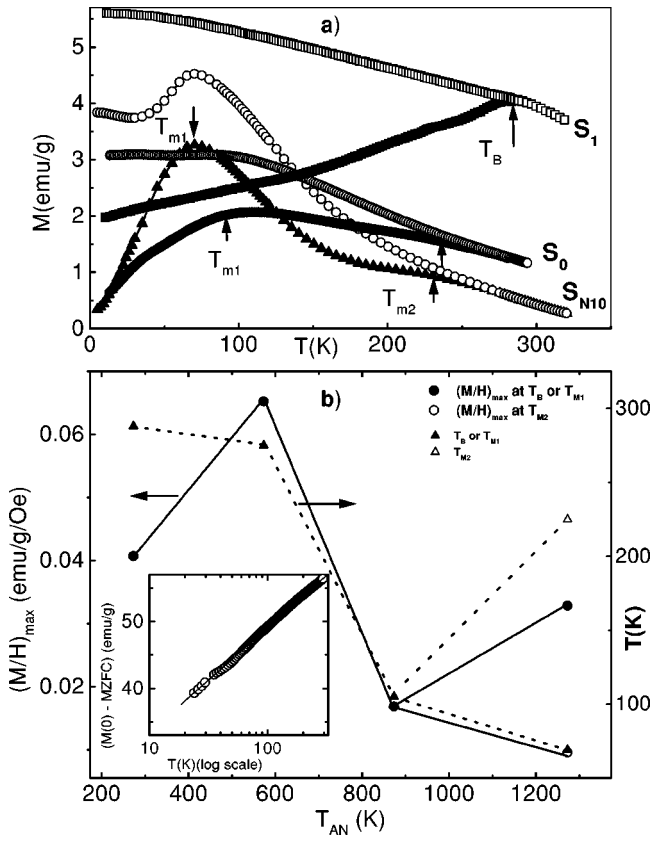

FIG. 2. (a) MZFC (solid) and MFC (open) vs temperature at 100 Oe for S_0, S_1, and S_{N10} samples. T_B: cluster blocking temperature, T_{m1}: cluster spin freezing temperature, T_{m2}: short-range ferrimagnetic ordering temperature. (b) Annealing temperature dependence of T_B, T_{m1}, and T_{m2} (right scale) and ZFC $(H/M)_{max}$ at T_B, T_{m1}, and T_{m2} (left scale). Lines guide to eye. Inset shows MZFC (solid) at 1 T along with fit data (line) to Bloch law.

the method of Le Caër and Dubois.[24] In this model a linear relationship between HMF (H) and isomer shift (IS) is assumed in the form $IS = aH + b$, where a and b are the fitting parameters to get the best fit. The IS is reported with respect to Fe metal.

III. RESULTS AND DISCUSSION

A. dc magnetization

Figure 2(a) shows the zero-field cooled magnetization (MZFC) and field cooled magnetization (MFC) at 100 Oe. The immediate result from Fig. 2(a) is that magnetic behavior of the as milled (S_1) sample is strikingly different from that of the bulk (S_0) sample in the following ways.

(1) The MZFC maximum at $T_{m1} \approx 100$ K (defined as the cluster spin-glass freezing temperature) and a small shoulder at $T_{m2} \approx 230$ K (defined as the short-range ferrimagnetic ordering temperature) seen for S_0 sample[21] disappear and a broad maximum of MZFC appears at $T_B \approx 280$ K for S_1 sample.

(2) An overall enhancement of magnetization (MZFC and MFC) in the temperature range 10–325 K is observed, when the S_0 sample is milled.

The MZFC magnetization data of S_1 sample show magnetic irreversibility and decrease, unlike the increase of MFC, below the temperature marked as T_B. The observation of prominent irreversibility for S_1 sample is either due to superparamagnetic blocking[25] or due to anisotropy (including strain induced) effect in the ferromagnetic clusters.[26] The other important features of the S_1 sample such as the field (H) dependence (not shown in figures) of $T_B(H)$ ~ 320 K (30 Oe), 280 K (100 Oe), and 20 K (1 T) indicate the superparamagnetic blocking of magnetic clusters.[25] Hence, T_B is defined as blocking temperature at a particular field.

In order to understand the coexistence of superparamagnetism with ferromagnetism in the as milled sample, we have analyzed the thermal (T) dependence of MZFC at 1 T field. We note for 1-T data that MFC values are nearly the same as MZFC values (not shown in Fig. 2) down to 10 K, except small magnetic irreversibility below 20 K. A polynomial fit of MZFC (T) data gives $M(0) \approx 55$ emu/g at 0 K. The inset of Fig. 2(b) dipicts that (M_0-MZFC) vs T at 1 T follows a magnon-type-Bloch law: $M(T) = M(0)(1 - AT^{\alpha})$. The best fit value of $\alpha = 1.55 \pm 0.01$ is larger in comparison to typical Bloch exponent $\alpha = 1.5$. We attribute the larger value of α to the (nano) particle size effect of the sample.[5,7] The application of Bloch law also implies that our as milled sample S_1 behaves as a ferromagnetic/ferrimagnetic system. Therefore, the observation of superparamagnetic behavior as well as the ferromagnetic/ferrimagnetic nature of the S_1 sample suggests that the particles of the S_1 sample are essentially ferromagnetic clusters showing superparamagnetic blocking below T_B due to its nanometer size.

We have measured $M(T)$ data for all the heat treated milled samples, but the results of S_{N10} sample only are shown in Fig. 2(a). The basic features of the results of all other heat treated milled samples are represented in Fig. 2(b). The MZFC(T) and MFC(T) plots (not shown) for other heat treated samples are similar to that of S_1 sample, but with blocking temperature T_B decreases to 270 K and 120 K for S_{N3} and S_{N6} samples, respectively. $M(T)$ of S_{N10} sample, which has $T_{AN} \approx 1273$ K, is more similar to that of the S_0 sample [Fig. 2(a)], but has a slightly different cluster spin-glass freezing temperature (T_{m1}) and short-range ferrimagnetic ordering temperature (T_{m2}). At 100 Oe, $T_{m1} \approx 70$ K and $T_{m2} \approx 225$ K for S_{N10} sample compared to $T_{m1} \approx 100$ K and $T_{m2} \approx 230$ K for S_0 sample. Interestingly, the MZFC maximum $(M/H)_{max}$ at T_B for S_{N3} sample shows further enhancement with respect to S_1 sample. Thereafter $(M/H)_{max}$ decreases for S_{N6} sample and again increases for the S_{N10} sample. This kind of nonequilibrium magnetic behavior reflects the refinement of grain boundary spins and reordering of cations by thermal activated process in mechanical milled spinel.[27] However, the magnitudes of $(M/H)_{max}$ at T_{m1} (~ 70 K) and T_{m2} (~ 225 K) for S_{N10} sample are larger and smaller than that of S_0 sample at T_{m1} (~ 100 K) and T_{m2} (~ 230 K), respectively. Thus, the heat treatment of milled sample at 1273 K for 6 h is not sufficient to restore the sample to the complete bulk properties.

The field (H) dependence of MZFC (Fig. 3, $T = 10$ K, 290 K) of S_1 sample is similar to that of ferromagnetic

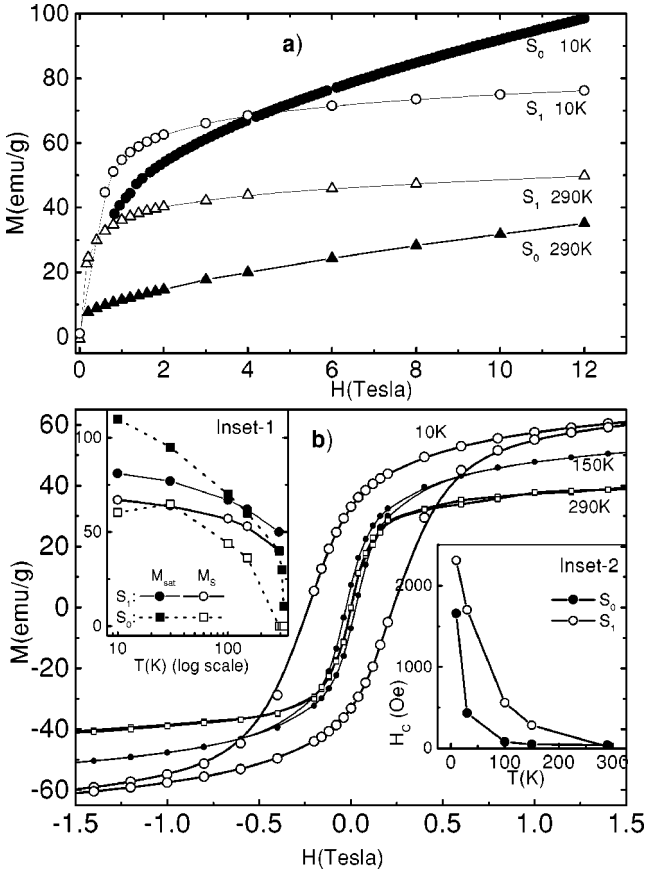

FIG. 3. (a) Magnetization vs field at 10 K and 290 K for S_0 and S_1 samples. (b) Hysteresis loops at selected temperatures for S_1 sample. Temperature dependence of saturation (M_{sat}), spontaneous (M_S) magnetization (inset 1) and coercive field (H_C) (inset 2) for S_0 and S_1 samples.

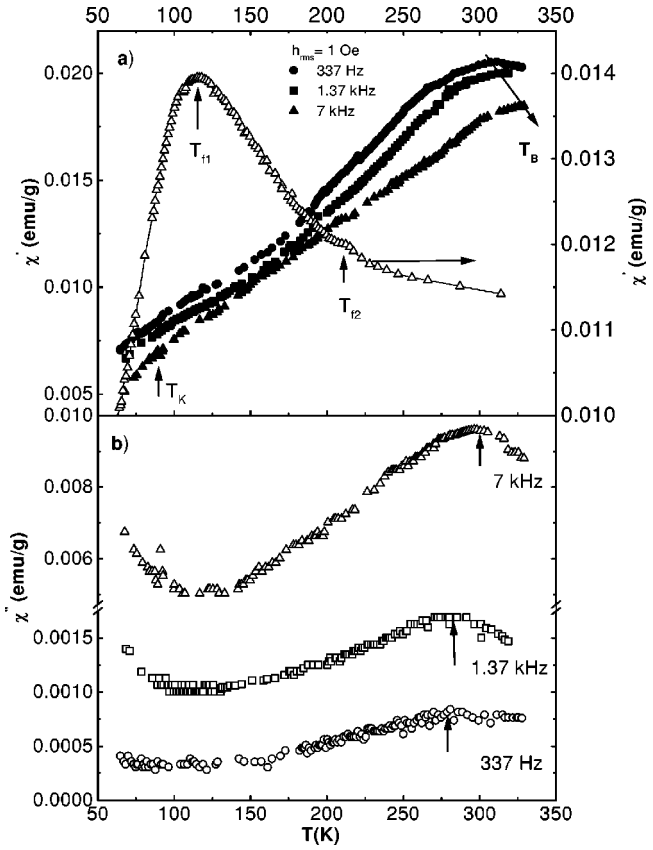

FIG. 4. ac susceptibity χ' (a) and χ'' (b) data for S_1 sample. T_K represents spin canting temperature. (a) right scale shows the χ' vs T data at 1 Oe, 337 Hz for S_0 sample. T_{f1} and T_{f2} represent lower and higher cluster spin freezing temperatures, respectively, for S_0 sample.

isotherm,[28] but the MZFC lacks saturation even up to 12 T. It is also noted that S_1 sample has a ''better ferromagnetic'' state with enhanced magnetization with respect to S_0 sample. However, the larger MZFC(H) of S_0 sample compared to that of S_1 sample at 10 K and high field ($H>4$ T) indicates that strong spin canting effect for bulk (S_0) sample[21] has been decreased by mechanical milling. On the other hand, the small increase of MZFC above 1 T of S_1 sample is due to the superparamagnetic contribution of nanoparticles.[8] To give further evidence of magnetic enhancement for S_1 sample, we have calculated saturation magnetization (M_{sat}) and spontaneous magnetization (M_S) using the law of approach to saturation (M vs $1/H$) and Arrot plot (M^2 vs H/M), respectively. The comparative data in Fig. 3(b) (inset 1) show that M_{sat} of S_0 sample is larger than S_1 sample, but spontaneous magnetization (M_S) of S_1 sample is enhanced with respect to S_0 sample. The larger value of M_{sat} is also consistent with the strong B site spin canting effect of bulk sample. The reduction of B site spin canting by mechanical milling is, further, proved by the observation of larger value of spontaneous magnetization (with better ferromagnetic order of spins) in the temperature range 10–300 K for S_1 sample. The $M(H)$ data of our as milled (S_1) sample are also remarkable in the following ways:

(1) Both saturation magnetization ($M_{sat}\sim 80$ emu/g) and spontaneous magnetization ($M_S\sim 67$ emu/g) at 10 K are larger than for the other mechanical milled spinels [$CdFe_2O_4\sim 21$ emu/g at 5 K,[16] $NiFe_2O_4\sim 55$ emu/g at 5 K (Ref. 17)] and even larger than that fo the mechanical milled $ZnFe_2O_4$ ($M_{sat}\sim 73$ emu/g) (Ref. 10).

(2) The above three spinels[10,16,17] have ordering temperature well below the room temperature, where as our as milled sample shows ordering even above room temperature and this is very important for possible room-temperature application of S_1 sample.

The magnetic ordering above 300 K for S_1 sample is due to small amount of Co^{2+} (~ 0.2) in our sample in comparison with $ZnFe_2O_4$. However, the observations of hysteresis loops [Fig. 3(b)] at 10 K and 150 K are typical of ferromagnetic, whereas the absence of hysteresis loop with zero coercive field (H_C) [Fig. 3(b), inset 2] at $T\geqslant 290$ K is further consistent with the superparamagnetic behavior of the ferromagnetic clusters.[28] It is to be noted that coercive field (H_C) of S_1 sample is larger than that of S_0 sample throughout the temperature below 300 K [Fig. 5(b),inset 2] and this definitely suggests the enhancement of unidirectional anisotropy in the as milled sample.[14] We, further, suggest that the strain induced anisotropy gives a preferential orientation to the grain boundary spins in our as milled sample.

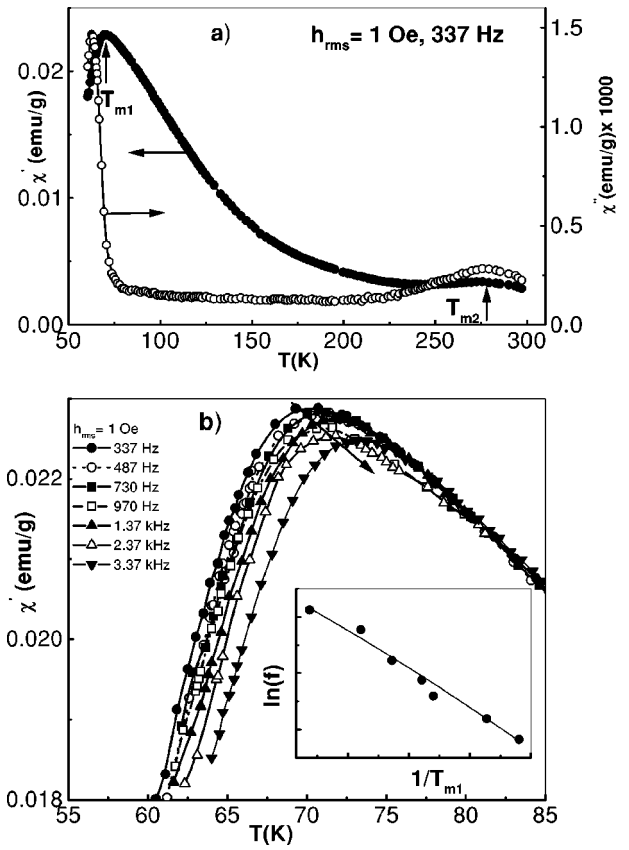

FIG. 5. (a) Temperature dependence of χ' (left scale) and χ'' (right scale) for S_{N10} sample. (b) shows χ' vs T about T_{m1} for f = 337 Hz to 7 kHz and corresponding ln(f) vs $1/T_{m1}$ plot (inset).

B. ac susceptibility

In order to better understand the spin dynamics, we have investigated the real (χ') and imaginary (χ'') components of ac susceptibility for S_1 sample and plotted in Fig. 4 along with χ' of S_0 sample. In addition to the enhancement of ac susceptibility χ', the ac response of S_1 sample (h_{rms} ~1 Oe, 337 Hz) shows two very striking differences with respect to the S_0 sample; viz., (1) the cluster spin freezing temperature at $T_{f1}\approx 110$ K for S_0 sample is highly suppressed to a small shoulder (designated as $T_K\sim 100$ K) in the S_1 sample and (2) the higher cluster-spin freezing temperature at $T_{f2}\sim 210$ K for S_0 sample shifts to considerably higher temperature ($T_B\sim 320$ K) for as milled (S_1) sample. The broad ac susceptibility maxima in S_1 sample suggest the cluster size distribution and reflect the associated relaxation time distribution in the sample.[1] The frequency f dependence of the χ' and χ'' maxima shows superparamagnetic blocking below $T_B(f)$. Thus, the broad maximum of χ' at $T_B \approx 320$ K corresponds to average blocking temperature of the ferromagnetic clusters. Since the χ' maximum is not well defined up to 325 K, we have calculated shift of T_B with f from maximum of χ''. The shift of T_B per decade of f [i.e., $\Delta T_B/T_B\Delta\ln(f)\approx 0.06$] is slightly less than the typical value of 0.1 for noninteracting superparamagnetic clusters and indicates certain degree of (ferromagnetic) interactions between the clusters.[12] However, the increasing tendency of χ'' [Fig. 2(b)] below T_K may indicate either the occurrence of maximum below T_K or the disorder effects of surface or grain boundary spins at low temperature.[9]

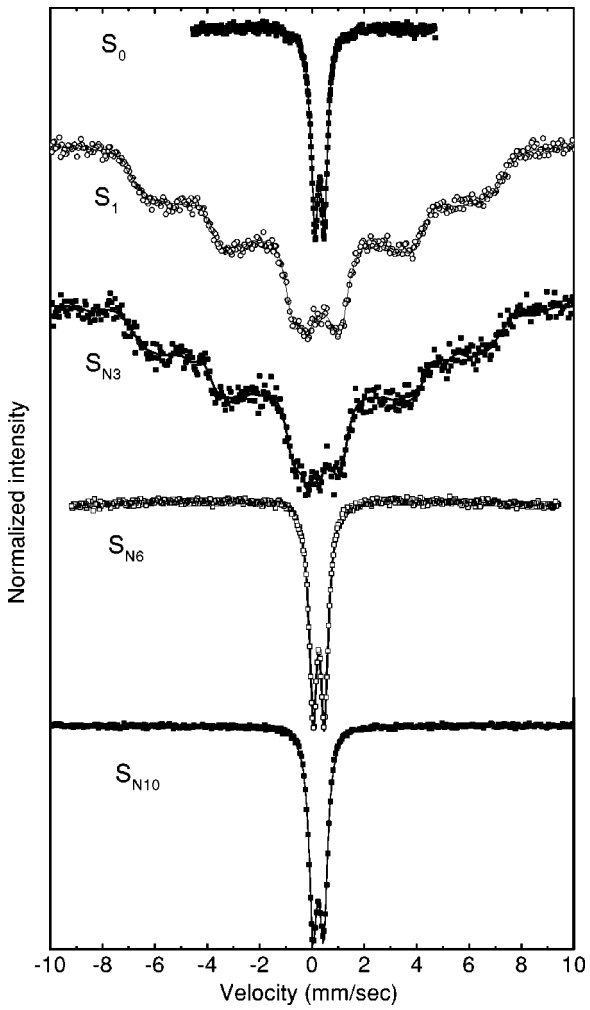

FIG. 6. Room-temperature Mössbauer spectra recorded in absence of field for S_0 and S_1, S_{N3}, S_{N6} and S_{N10} samples.

The ac susceptibility data, with two distinct maxima, in Fig. 5(a) for S_{N10} sample are considerably different from those of S_0 sample [χ' in Fig. 4(a)]. The χ' and χ'' maxima of S_{N10} sample at $T_{m2}\approx 280$ K exhibit a very small frequency (range: from 337 Hz to 7 kHz) dependence (not shown in figure), which shows the appearance of short-range ferrimagnetic order of bulk at $T_{m2}\approx 260$ K.[21] The low-temperature χ' maximum at $T_{m1}\approx 70$ K and the sudden onset of χ'' maximum at the inflection point (~ 63 K) of χ' vs T data are essentially the cluster spin-glass freezing, but in a refined manner with respect to the bulk sample.[21] The occurrence of cluster spin-glass freezing of S_{N10} sample at lower temperature comparing the bulk sample is attributed to the smaller particle size effect. The T_{m1} has a significant positive frequency dependence for both χ' [Fig. 5(b)] and χ'' (not shown in figure), as has been observed earlier in other mechanical milled samples.[11,12,29] The frequency shift of T_{m1} follows Vogel-Fulcher law [Fig. 5(b), inset]:

$$f = f_0 e^{-E_a/(T_{m1}-T_0)} \quad (1)$$

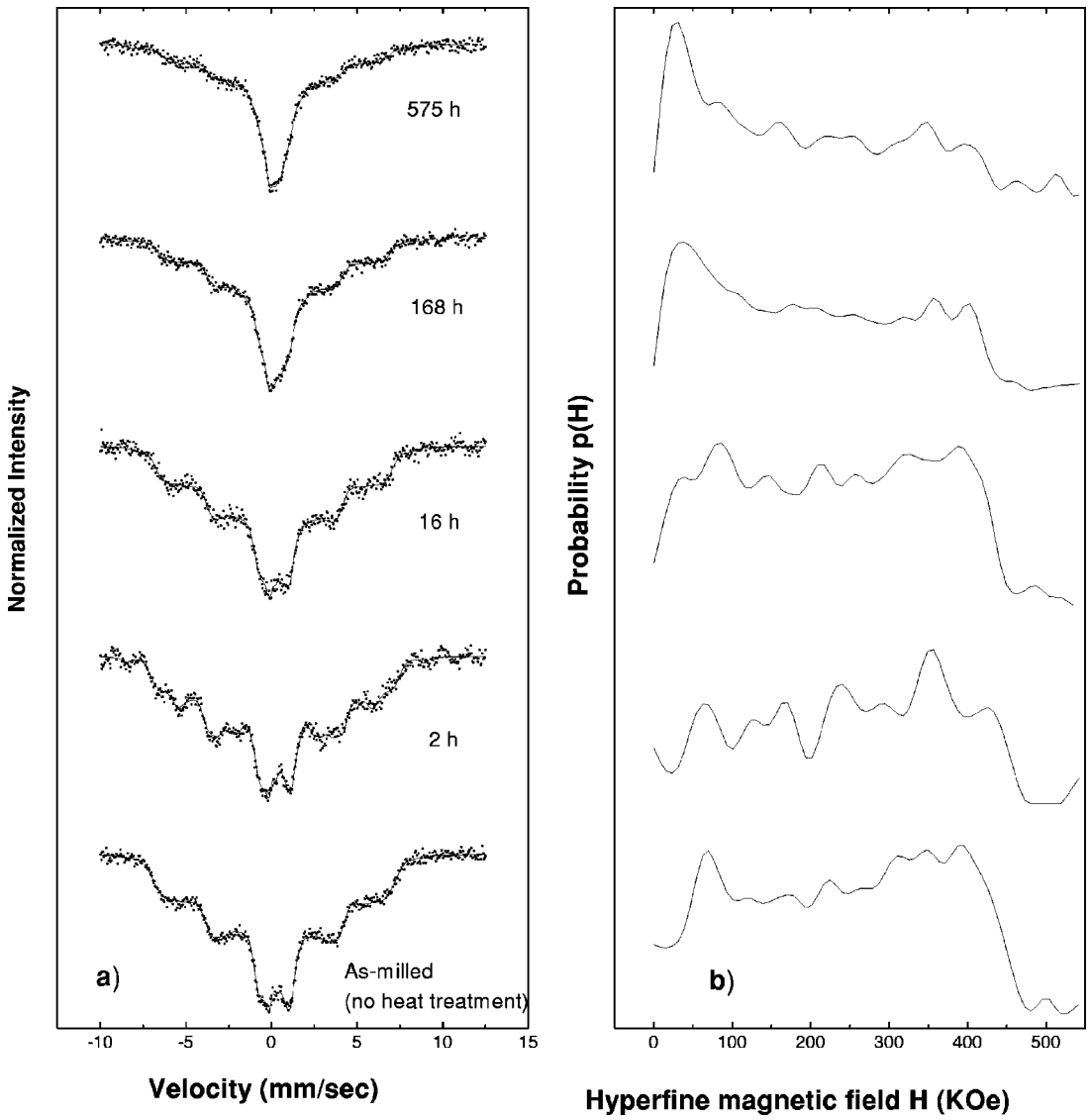

FIG. 7. Room-temperature Mössbauer spectra for heat treated $Co_{0.2}Zn_{0.8}Fe_2O_4$ sample at 573 K for different annealing time (t_{AN}) (a) and corresponding hyperfine field distribution (b).

with characteristic frequency $f_0 \approx 10^{10}$ Hz, activation energy $E_a \approx 379$ eV, and constant $T_0 \approx 47$ K. The corresponding frequency shift per decade of f [i.e., $\Delta T_{m1}/T_{m1}\Delta \ln(f) \approx 0.05$] is consistent with spin-glass behavior in $ZnCr_{1.6}Ga_{0.4}O_4$ spinel oxide[30] and is close to the cluster spin-glass value of bulk sample (≈ 0.044).[21] The finite value of $T_0(\approx 47$ K), again, suggests interactions between clusters via grain boundary spins.

C. Mössbauer spectroscopy

Besides the macroscopic probes such as dc magnetization and ac susceptibility, Mössbauer spectroscopy is an important tool to probe for local information of magnetization such as hyperfine field distribution, cations ordering through grain growth kinetics of mechanical milled sample.[10,17,22] Figure 6 shows the room-temperature Mössbauer spectra of as prepared bulk (S_0), as milled (S_1), and heat treated S_{N3}, S_{N6}, and S_{N10} samples. The spectrum of S_0 sample consists of a Lorentzian doublet arising from the Fe^{3+} ions at octahedral (B) sites and a Lorentzian singlet arising from the Fe^{3+} ions at tetrahedral (A) sites. The intensity ratio of the paramagnetic doublet and a singlet was nearly 9:1, which corresponded very well with the most probable cation distribution of the form $(Zn_{0.8}Fe_{0.2})_A[Co_{0.2}Fe_{1.8}]_BO_4$.[20] The presence of only a paramagnetic doublet in the Mössbauer spectrum is consistent with the results of magnetization measurement of S_0 sample [Fig. 2(a)] showing the irreversibility between ZFC and FC magnetizations below 260 K. The IS and quadrupole splitting (QS) of Fe^{3+} ions at [B] site are $\approx +0.29$ mm/sec and 0.35 mm/sec, respectively. The IS value of Fe^{3+} ions at (A) site is ≈ -0.056 mm/sec. These values are in very good agreement with the range of IS and QS values reported in case of Zn and Ni ferrites.[15,17] The Mössbauer spectrum, therefore, confirms that the as prepared bulk $Co_{0.2}Zn_{0.8}Fe_2O_4$ sample is in a perfect cation ordered state where Zn^{2+} occupies A site, Co^{2+} prefers B site, and Fe^{3+}

shares both *A* and *B* sites. The IS and QS values obtained also confirm the presence of only Fe^{3+} charge state and not Fe^{2+} charge state in the system.

The Mössbauer spectrum (Fig. 6) of the S_1 sample clearly indicates the ferromagnetic hyperfine splitting at room temperature in addition to a central paramagnetic doublet. We explain the increased ferromagnetic interaction due to site exchange of Zn^{2+} and Fe^{3+} ions by mechanical milling. The site exchange brings about an increase in the number of Fe^{3+} ions at *A* site.[10,15] This increases the intersublattice exchange interactions J_{AB} (Fe_A^{3+}-O^{2-}-Fe_B^{3+}), which further decrease the *B* site spin canting.[3] Mechanical milling may also modify the *B* sublattice exchange interactions J_{BB} (Fe_B^{3+}-O^{2-}-Fe_B^{3+}) by deforming the *B* site bond angle different from 90° (typical of the bulk sample).[31] Thus, the ordered cation distribution of S_0 sample is destroyed and a nonequilibrium (disorder) cation distribution appears due to mechanical milling. Consequently, ferromagnetic/ferrimagnetic order is enhanced above room temperature. The relaxation effects observed in the room-temperature Mössbauer spectrum of S_1 sample, further, confirm the superparamagnetic blocking due to nanosize clusters (grains).[10,17] By increasing the annealing temperature (T_{AN}), the hyperfine magnetic field splitting decreases and paramagnetic doublet increases, as seen for S_{N6} and S_{N10} samples. Even though the Mössbauer spectrum of S_{N10} and S_0 samples seem to be similar, but the fitted parameters (IS$=+0.27$ mm/sec and QS$=+0.43$ mm/sec for *B* site Fe^{3+} ions and the IS$=+0.25$ mm/sec of *A* site Fe^{3+} ions) of S_{N10} sample differ from that of the S_0 sample. This suggests that 6 h heat treatment at 1273 K is not enough to achieve 100% equilibrium cation ordering of the bulk sample.

In order to describe qualitatively the cation reordering kinetics, we have shown [Fig. 7(a)] the Mössbauer spectra of heat treatment (at 573 K) of as milled sample as a function of annealing time (t_{AN}). The corresponding HMF distribution [$p(H)$] is shown in Fig. 7(b). The peaks in the distribution [Fig. 7(b)] correspond to HMF seen by the Fe^{3+} ions at *B* sites with a nonuniform environment, consisting of different numbers of Zn^{2+} and Fe^{3+} ions at the nearest-neighbor *A* sites. The HMF experienced by Fe^{3+} ions at *A* sites remains unaffected by the nearest-neighbor *B* site configuration.[32] It is observed that the shape of $p(H)$ distribution is not changed significantly after 2 h of heat treatment, except the distinct peaks at higher field values are merging to give a broad peak. We, therefore, increase the annealing time (t_{AN}) up to 575 h. It is clear for $t_{AN} \geqslant 16$ h that the $p(H)$ intensities of lower field components are increasing at the expense of higher field components. On the other hand, the Mössbauer spectra [Fig. 7(a)] show that paramagnetic component, near zero velocity, increases and hyperfine field splitting at higher velocity decreases with $t_{AN} \geqslant 16$ h. The paramagnetic component in the heat treated samples could be attributed to the superposition of a doublet due to Fe^{3+} ions at *B* sites and of a singlet due to Fe^{3+} ions at *A* sites. Indirectly, the increase of paramagnetic component gives the information that more and more number of Zn^{2+} ions are stabilizing at *A* sites with the equal number of Fe^{3+} ions at *B* sites. This means that cation reordering is taking place as a function of t_{AN}.

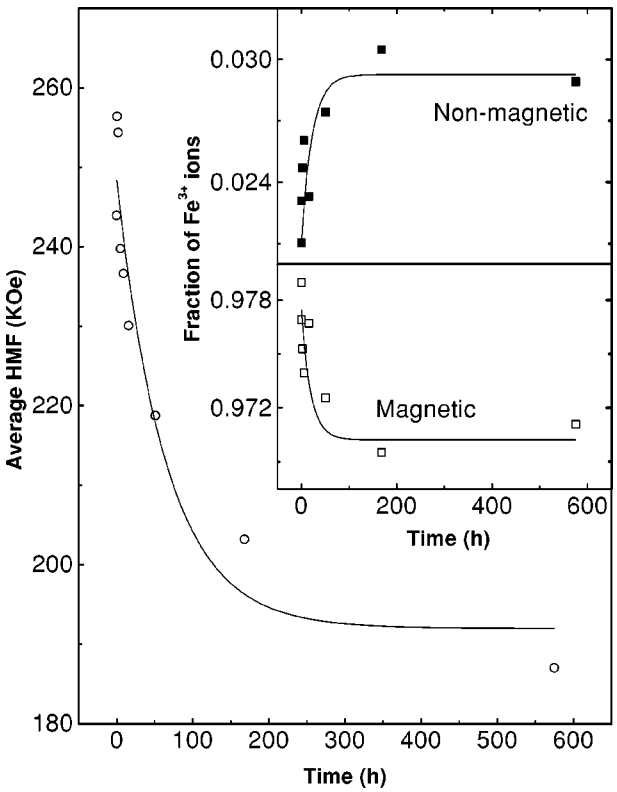

FIG. 8. Annealing time (t_{AN}) dependence of average hyperfine field value (main panel) and fraction of magnetic and nonmagnetic Fe^{3+} ions (inset) for the as milled $Co_{0.2}Zn_{0.8}Fe_2O_4$ sample, annealing was performed at 573 K.

The small nonmagnetic fraction present, even, in the Mössbauer spectrum of as milled sample shows that complete site disorder was not achieved and there was some residual cation ordering after 24 h milling. Therefore, we used the method of Le Caër and Dubois[24] to evaluate the intensities of the magnetic and nonmagnetic fractions by fitting the Mössbauer spectra. We have introduced two fixed zero-field components with QS and IS characteristics of Fe^{3+} ions at *A* and *B* sites of as prepared bulk sample to fit the central doublet apart from the HMF distribution. Figure 8 shows the temporal evolution of the average HMF (main panel) along with magnetic and nonmagnetic fractions (Fig. 8, inset) at 573 K. The magnetic fraction refers to the total area of the superparamagnetically split spectrum and the nonmagnetic fraction refers to the area of the paramagnetic doublet. The solid lines represent the fit data using an exponential function: $F(t)=a\pm b[1-\exp(t_{AN}/t_0)]$ where $\pm$ refers to increasing or decreasing functions and *a*, *b*, t_0 are constants. $F(t)$ represents average HMF, and magnetic and nonmagnetic fractions as a function of annealing time (t_{AN}). The continuous decrease of magnetic fraction along with average HMF is associated with an increase in the nonmagnetic fractions, i.e., paramagnetic component in the sample at 300 K. The good quality of fit to the data (Fig. 8) shows the linear response of grain growth kinetics through the grain boundary atomic diffusion during heat treatment.[22] The rapid decrease

of magnetic fraction for $t_{AN} \geqslant 100$ h can be related to the fast relaxation of mechanically induced microstrain in the lattices during slow grain growth process.[22] The observation of clear hyperfine splitting even after 575 h annealing suggests that particle (grain) size slowly increases with t_{AN} at 573 K. The nonlinear grain growth occurs only when annealing temperature increases above 573 K, as seen from paramagnetic spectrum of S_{N6} and S_{N10} samples. Therefore, the cation reordering kinetics is also related to the thermal activated grain boundary mobility with annealing time (t_{AN}) and temperature (T_{AN}).

IV. CONCLUSIONS

The present study conclusively shows the following results.

(1) The enhancement in both magnetization and ferromagnetic/ferrimagnetic order is intrinsic property of the mechanical milled $Co_{0.2}Zn_{0.8}Fe_2O_4$ nanoparticle. This system is one of the few spinels, which shows magnetic enhancement by mechanical milling.

(2) The enhancement in ferromagnetic/ferrimagnetic order is attributed to the site exchange of cations (Zn^{2+} and Fe^{3+}) among the *A* and *B* sites by mechanical milling. Except the site exchange of cations, we correlate the enhancement of magnetization of nanoparticle to the inverse of spin canting effect, i.e., the lowering of *B* site spin canting by milling of bulk sample causes the enhancement of magnetization. To our knowledge, this is the first report which highlights the importance of inverse of spin canting effect for mechanical milled nanoparticle spinel.

(3) The enhancement of coercive field in mechanical milled sample comparing the bulk sample throughout the temperature below 300 K is attributed to the (mechanical) strain induced anisotropy, which further gives rise to preferential orientation of the grain boundary spins.

(4) The coexistence of superparamagnetism with ferromagnetism in the as milled sample arises due to particle (nano) size effect.

(5) The milled sample requires long annealing time at higher temperature ($\sim$1273 K) for the recovery of ordered cation distribution of the bulk sample.

(6) Finally, the large magnetic moment and ordering temperature near to room temperature of the mechanical milled $Co_{0.2}Zn_{0.8}O_4$ may be considered for the possible nanotechnological application of this material.

ACKNOWLEDGMENTS

One of the authors (R.N.B.) acknowledges Council of Scientific and Industrial Research (CSIR, India) for financial support [Grant No. F.No.9/489(30)/98-EMR-I].

*Email address: rnb@cmp.saha.ernet.in

†Email address: ranga@cmp.saha.ernet.in

[1] *Magnetic Properties of Fine Particles*, edited by J.L. Dorman and D. Fiorani (North-Holland, Amsterdam, 1991).

[2] R.C. Handley, *Modern Magnetic Materials: Principles and Applications* (Wiley, New York, 2000).

[3] V.A.M. Brabers, in *Handbook of Magnetic Materials*, edited by K.H. Buschow (North-Holland, Amsterdam, 1995), Vol. 8 p. 189; S. Krupika and P. Novak, in *Ferromagnetic Materials*, edited by E.P. Wolfarth (North-Holland, Amsterdam, 1982), Vol. 3 p. 189.

[4] R.H. Kodama and A.E. Berkowitz, Phys. Rev. B **59**, 6321 (1999).

[5] Xavier-Batlle and A. Labarta, J. Phys. D **35**, R15 (2002).

[6] D.J. Fatemi, V.G. Harris, M.X. Chen, S.K. Malik, W.B. Yelon, G.J. Long, and A. Mohan, J. Appl. Phys. **85**, 5172 (1999).

[7] J.P. Chen, C.M. Sorensen, K.J. Klabunde, G.C. Hadjipanayis, E. Devlin, and A. Kostikas, Phys. Rev. B **54**, 9288 (1996).

[8] G.F. Goya and H.R. Rechenberg, J. Phys.: Condens. Matter **10**, 11 829 (1998); G.F. Goya, H.R. Rechenberg, and J.Z. Jiang, J. Magn. Magn. Mater. **218**, 221 (2000).

[9] R.H. Kodama, A.E. Berkowitz, E.J. McNiff, Jr., and S. Foner, Phys. Rev. Lett. **77**, 394 (1996).

[10] H.H. Hamdeh, J.C. Ho, S.A. Oliver, R.J. Willey, G. Oliveri, and G. Busca, J. Appl. Phys. **81**, 1851 (1997); S.A. Oliver, V.G. Harris, H.H. Hamdeh, and J.C. Ho, Appl. Phys. Lett. **76**, 2761 (2000).

[11] G.F. Zhou and H. Bakker, Phys. Rev. Lett. **72**, 2290 (1994).

[12] J.A. De Toro, M.A. Lopez de la Torre, J.M. Riveiro, R.Sacz. Puche, A. Gomez-Herrero, and L.C. Otero-Diaz, Phys. Rev. B **60**, 12 918 (1999).

[13] J.A. De Toro, M.A. Lopez de la Torre, J.M. Riveiro, J. Bland, J.P. Goff, and M.F. Thomas, Phys. Rev. B **64**, 224421 (2001).

[14] Y. Shi and J. Ding, J. Appl. Phys. **90**, 4078 (2001).

[15] C.N. Chinnasamy, A. Narayanasamy, N. Ponpandian, K. Chattopadhyay, H. Gueralt, and J.-M. Greneche, J. Phys.: Condens. Matter **12**, 7795 (2000).

[16] C.N. Chinnasamy, A. Narayanasamy, N. Ponpandian, R.J. Joseyphus, K. Chattopadhayay, K. Shinoda, B. Jeyadevan, K. Tohji, K. Nakatsuka, and J.-M. Greneche, J. Appl. Phys. **90**, 527 (2001).

[17] C.N. Chinnasamy, A. Narayanasamy, N. Ponpandian, K. Chattopadhyay, K. Shinoda, B. Jeyadevan, K. Tohji, K. Nakatsuka, T. Furubayashi, and I. Nakatani, Phys. Rev. B **63**, 184108 (2001).

[18] V.A.M. Brabers, Phys. Rev. Lett. **68**, 3113 (1992).

[19] P.J. van der Zaag, A. Noordermeer, M.T. Johnson, and P.F. Bongers, Phys. Rev. Lett. **68**, 3112 (1992).

[20] G.A. Petitt and D.W. Forester, Phys. Rev. B **4**, 3912 (1971).

[21] R.N. Bhowmik and R. Ranganathan, J. Magn. Magn. Mater. **248**, 101 (2002).

[22] C.E. Krill III, L. Helfen, D. Michels, H. Natter, A. Fitch, O. Masson, and R. Birringer, Phys. Rev. Lett. **86**, 842 (2001).

[23] Anindita Ray, A. Chakravarti, and R. Ranganathan, Rev. Sci. Instrum. **67**, 789 (1996); A. Chakravarti, R. Ranganathan, and A.K. Raychaudhuri, Pramana, J. Phys. **36**, 231 (1991).

[24] G. Le Caër and J.M. Dubois, J. Phys. E **12**, 1083 (1979).

[25] Qi Chen and Z.J. Zhang, Appl. Phys. Lett. **73**, 3156 (1998).

[26] S. Mukherjee, R. Ranganathan, P.S. Anil Kumar, and P.A. Joy, Phys. Rev. B **54**, 9267 (1996).

[27] A.E. Berkowitz, J.A. Lahut, and C.E. VanBuren, IEEE Trans. Magn. **16**, 184 (1980).

[28] M. Muroi, R. Street, P.G. McCormick, and J. Amighian, Phys. Rev. B **63**, 184414 (2001).

[29] D.X. Li, K. Sumiyama, K. Suzuki, and T. Suzuki, Phys. Rev. B **55**, 6467 (1997).

[30] D. Fiorani, S. Viticoli, J.L. Dormann, J.L. Tholence, and A.P. Murani, Phys. Rev. B **30**, 2776 (1984).

[31] V. Sepelak, S. Wißmann, and K.D. Becker, J. Magn. Magn. Mater. **203**, 135 (1999).

[32] H.M. van Noort, J.W.D. Martens, and W.L. Peeters, Mater. Res. Bull. **20**, 41 (1985).